Journal of Asian Ceramic Societies

ISSN: (Print) (Online) Journal homepage: https://www.tandfonline.com/loi/tace20

Surface and volume crystallization in fluorrichterite based glasses

R. Casasola , J. M. Pérez & M. Romero

To cite this article: R. Casasola , J. M. Pérez & M. Romero (2020) Surface and volume crystallization in fluorrichterite based glasses, Journal of Asian Ceramic Societies, 8:3, 642-652, DOI: 10.1080/21870764.2020.1770939

To link to this article: https://doi.org/10.1080/21870764.2020.1770939

Published online: 26 May 2020.

JOURNAL OF ASIAN CERAMIC SOCIETIES
2020, VOL. 8, NO. 3, 642–652
https://doi.org/10.1080/21870764.2020.1770939

THE CERAMIC SOCIETY OF JAPAN
THE KOREAN CERAMIC SOCIETY
Taylor & Francis
Taylor & Francis Group

FULL LENGTH ARTICLE

Surface and volume crystallization in fluorrichterite based glasses

R. Casasola, J. M. Pérez and M. Romero

Group of Glass and Ceramic Materials, Materials Department, Eduardo Torroja Institute for Construction Sciences (Ietcc-csic), Madrid, Spain

ABSTRACT

F-richterite based glasses in the SiO_2-CaO-MgO-Na_2O-F system were investigated by X-ray diffraction, differential scanning calorimetry and field emission scanning electron microscopy to ascertain the influence of fluorine content on preferential crystallization mechanism and on the spatial position of crystals developed in the initial steps of glass devitrification. The results highlight that both surface and volume mechanisms occur in the crystallization of fluorrichterite glasses. However, these glasses preferentially devitrify by a surface crystallization mechanism, although an increase of fluorine content leads to a modification in the location of the first developed crystals.

ARTICLE HISTORY
Received 21 February 2020
Accepted 13 May 2020

KEYWORDS
F-richterite; DSC; crystallization mechanism; surface crystallization; bulk crystallization; microstructure

1. Introduction

Glass-ceramics are ceramic materials developed through the controlled crystallization (nucleation and crystal growth) of a glass. Given that the main glass-forming systems are based on silicates compositions, the major crystalline phases in glass-ceramics are also silicates [1]. Among crystalline silicates of interest in glass-ceramics, inosilicates or chain silicates are a silicate group whose structure is characterized by the arrangement of silicate tetrahedra in chains. Single chains ($[Si_nO_{3n}]^{2n-}$), double chains ($[Si_{4n}O_{11n}]^{6n-}$) and even complex chains are feasible. Minerals belonging to the inosilicate group include the pyroxenes (single chain) and the amphiboles (double chain) [2].

A general amphibole formula may be written as $A_{0-1}B_2C_5(Si,Al)_8O_{22}(OH,F)_2$ where the most common cations are: A: Na, K; B: Na, Ca, Mg, Fe^{2+}; C: Mg, Fe^{2+}, Al, Fe^{3+}. Glass-ceramic materials comprising amphibole minerals can enclose one or more of K-fluorrichterite ($KNaCaMg_5Si_8O_{22}F_2$), fluorcanasite ($K_2Na_4Ca_5Si_{12}O_{30}F_4$) and agrellite ($NaCa_2Si_4O_{10}F_2$) crystalline phases [3]. The microstructure of fluor-amphibole glass-ceramics consists of arbitrarily faced needle-shaped crystals, encouraging several crack deflections when cracked. Glass-ceramics in this system are distinguished by high values of flexural strength and fracture toughness, as well as excellent acid and alkali chemical durability [3,4].

Fluorrichterite glass-ceramics have already found commercial applications as high-performance tableware (Pyroceram© and Corelle© brands). However, in spite of their outstanding technological properties, there is a lack of scientific data on fluorrichterite glass-ceramics since the literature on this subject is limited to few papers reported on the preparation of oriented fuorrichterite/diopside glass-ceramics by electrochemically induced nucleation [5]; the effect of crystallization heat treatment on the microstructure and flexural strength of fluorrichterite glass-ceramics [6]; the study of their crystallization behavior [7–9] and of the feasibility of using fluorrichterite glass-ceramics as biomaterials, such as heat-pressed dental ceramics [4,10,11], glass-ceramics with osteoconductive potential [12–15] or glass-ceramics suitable for hard tissue augmentation [16].

However, limited papers report on the progress of crystals at the earliest stage of the devitrification of fluorrichterite. In previous papers, we stated the concurrence of surface and bulk crystallization in the devitrification process of Na-fluorrichterite glasses [17]. Surface crystallization mechanism predominates at the beginning of the crystallization process; however, volume crystallization attains significance with increasing fluorine content in glass composition [18]. The purpose of the present paper is to studythe crystal growth in the initial steps of devitrification of glasses belonging to the SiO_2-CaO-MgO-Na_2O-F system with variable fluorine content.

2. Experimental

A glass with the stoichiometric composition of fluorrichterite, $Na_2CaMg_5Si_8O_{22}F_2$ and from now on labeled as RE glass, was studied in the SiO_2-CaO-MgO-Na_2O-F system and synthesized from silica sand with low contents of iron oxide and reagent grade $(MgCO_3)_4Mg(OH)_2.5H_2O$, $CaCO_3$, Na_2CO_3 and MgF_2. In base to RE composition, three additional glass compositions

CONTACT M. Romero mromero@ietcc.csic.es Group of Glass and Ceramic Materials, Materials Department, Eduardo Torroja Institute for Construction Sciences (Ietcc-csic), C/ Serrano Galvache 4, Madrid 28033, Spain

with 6, 8 and 10 wt.% of fluorine were formulated. They were labeled as R6, R8, and R10, respectively.

The raw materials mixtures were homogenized in a planetary ball mill (TURBULA, WAB-GROUP, Switzerland) for 15 min. The batches were melted at 1450ºC for 2 h in an electric furnace. Alumina-silica crucibles were used to contain the melts. After homogenization, melts were cooled in two different ways in order to get glasses as bulk or frit form. Thus, bulk glasses were obtained by pouring the melt on a brass mold. In order to minimize residual stress and to avoid glass devitrification, bulk glasses were annealed at a temperature of T_g-100ºC for 2 hours. For each glass composition, T_g was previously determined from differential scanning calorimetry (DSC) on glass samples with the same chemical composition (18). The T_g values determined for the RE, R6, R8 and R10 glasses are 565º, 560º, 550º and 535ºC respectively. On the other hand, frit glasses were obtained by pouring the melts into cool water.

The chemical analysis of the resulting glasses was determined by X-ray fluorescence (XRF)(BRUCKER S8 Tiger spectrometer, USA) The analysis was performed on pressed pellets of powder glass samples (<63 µm).

The crystallization mechanism study was conducted by both DSC and field emission scanning electron microscopy (FESEM). DSC study (SETARAM Labsys Thermal Analyzer, France) was carried out on samples with two different particle sizes, i.e., fine (< 63 µm powder) and coarse (~ 3 × 3 x 4 mm fragment). The samples were heated under flowing air from room temperature to 1400ºC at a heating rate of 50ºC·min^{-1}. Samples of 40 mg were placed in platinum crucibles and calcined Al_2O_3 was used as the reference material. All the DSC curves were normalized with respect to the sample weight.

For corroborating the preferential crystallization mechanism (surface or volume), the beginning of crystal growth was promoting by subjecting fragment samples of parent glasses to thermal treatments at the temperature interval 800–1100ºC for 5 min. For each composition, the pair (temperature, time) that results in the minimum crystal development that can be detected by XRD were selected. To carry out the crystallization treatments, the glass fragments were placed in the furnace, previously heated at the treatment temperature. After 5 min, the samples were taken out of the furnace and air-cooled. The microstructure of the subsequent glass-ceramic materials was examined by FESEM (HITACHI S-4800P microscope, Japan) using an acceleration voltage of 20 kV. Samples were polished to a 1 µm finish using diamond pastes after initially grinding with SiC powder. The samples were subsequently etched for 10 s in a solution of 5% HF, ultrasonically washed with distilled water and ethylic alcohol, dried and coated with Au-Pd (Balzers SCD 050 sputter, Lienchestein). Semi-quantitative analysis of the different phases was performed by energy-dispersive X-ray spectroscopy (EDS) with a Link eXL detector provided by a beryllium (Be) window.

The amorphous character of the as-melted glasses and the mineralogical analysis of the crystalline phases devitrified after thermal treatment was accomplished using X-ray diffraction (XRD) (BRUKER D8 Advance equipment with Ni-filtered Cu Kα radiation, USA) at 30 mA and 40 kV. Data were recorded in the 5–60° 2Θ range (step size 0.019732º and 0.5 s counting time for each step).

3. Results

After batch melting and homogenization, both cooling approaches (bulk or frit form) lead to glasses with homogeneous appearance and free of macroscopic defects, such as bubbles or crystalline inclusions. The X-ray diffraction study shows that, regardless of the cooling method followed in their manufacture, the resulting materials are entirely amorphous since their diffractograms exhibit a shapeless halo in the range 2θ = 20–40º, which is indicative of glassy materials. In all cases, the lack of diffraction peaks reveals the absence of crystalline phases formation during cooling. As an example, Figure 1 shows the XRD pattern of R10 glass prepared in bulk form by pouring the melt on a mold.

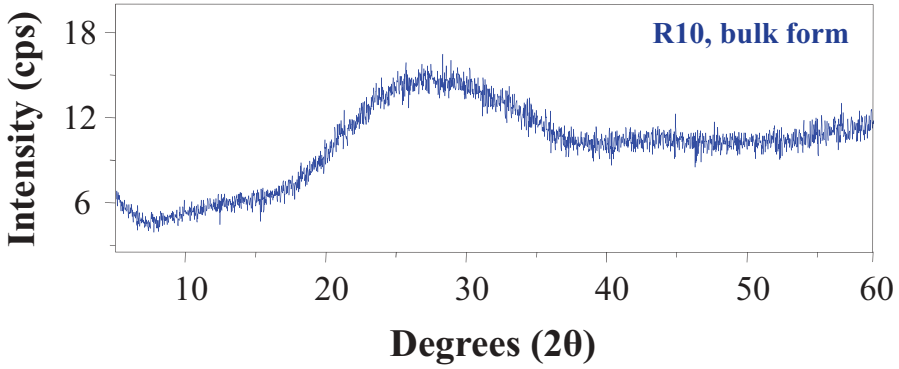

Figure 1. XRD pattern of R10 glass prepared in bulk form by pouring the melt on a mold.

Table 1. Experimental (XRF) chemical composition (wt.% in elements and expressed as oxides) of the investigated glasses. The error is approximately ± 0.2 wt%.

	RE	R6	R8	R10		RE	R6	R8	R10
Si	27.0	26.9	26.1	26.1	SiO_2	57.7	57.5	55.9	55.7
Al	2.8	3.6	4.2	4.6	Al_2O_3	5.3	6.8	7.9	8.7
Mg	12.6	12.3	12.0	11.6	MgO	20.9	20.3	20.0	19.2
Ca	5.6	5.1	4.9	4.8	CaO	7.8	7.1	6.8	6.7
Na	4.6	4.2	4.0	3.9	Na_2O	6.2	5.6	5.4	5.3
F_2	2.1	2.8	4.0	4.4	F^-	2.1	2.8	4.0	4.4
O	45.4	45.3	44.7	44.7					

Table 1 shows the chemical composition of the investigated glasses determined by X-ray fluorescence. In the course of the melting process, the molten glass is enriched in silica and alumina due to corrosion of the melt against the walls of the silica-alumina refractory crucibles used in the melting of raw materials mixtures [19]. Simultaneously, the fluorine percentage is reduced to a greater extent due to its volatilization as SiF_4 [20].

The thermal behavior of glasses was evaluated by DSC in samples with two different particle sizes, i.e., fine and coarse. As an example, Figure 2 shows the DSC curves recorded from powder and fragment samples of R10 glass prepared in bulk form. Independently of both cooling step (pouring on mold or on cool water) and particle size (fine or coarse) of glass sample, the DSC curves show one exothermic peak indicating that subsequent heat treatments could lead to the glass devitrification. The thermal stability of the glasses can be evaluated from the relative positions of the characteristic temperatures, viz. T_g (glass transition temperature), T_x and T_p (onset and peak crystallization temperatures, respectively), and T_m (melting temperature) [18,21]. Thus, the reduced glass transition temperature T_{gr} ($T_{gr} = T_g/T_m$) is indicative of the crystallization mechanism [22]. A value of $T_{gr} < 0.58$ indicates that crystals developed after thermal treatment will be homogeneously and randomly disseminated all over the whole glass body (volume crystallization) whereas when $T_{gr} > 0.60$ crystals mainly develop at the glass surface and subsequently grow into the glass volume [23,24]. On the other hand, ΔT_p is described as the difference between T_p in fine glass sample and T_p in coarse glass sample, $\Delta T_p = T_p(\text{fine}) - T_p(\text{coarse})$ [25]. The values of this parameter definitely help us to predict whether the crystallization process will start in surface or inside the glass particles. Thus, when $\Delta T_p > 0$ crystals will start growing preferably in the internal volume of the glass particles. On the contrary, when $\Delta T_p < 0$, the first crystals will be formed on the glass particle surfaces.

Table 2 collects the T_{gr} and ΔT_p values determined from DSC characteristic temperatures. The differences observed in the ΔT_p values between glasses prepared in frit or bulk form are associated with the different degree of packing of the molecules during the cooling of the melt. If the cooling is very fast (frit) the packing is lower and consequently, frit glasses will show lower T_g, T_m and especially T_p values than bulk glasses. Consequently, glasses prepared in frit or bulk form will also show different ΔT_p values. T_{gr}values suggest that the crystallization mechanism is weakly affected by the fluorine content in glass composition and surface crystallization mechanism is slightly prevalent since $T_{gr} > 0.60$ for all glasses in the series. However, T_{gr} values are close to 0.58–0.60 range, which demarcates the edge between surface and volume

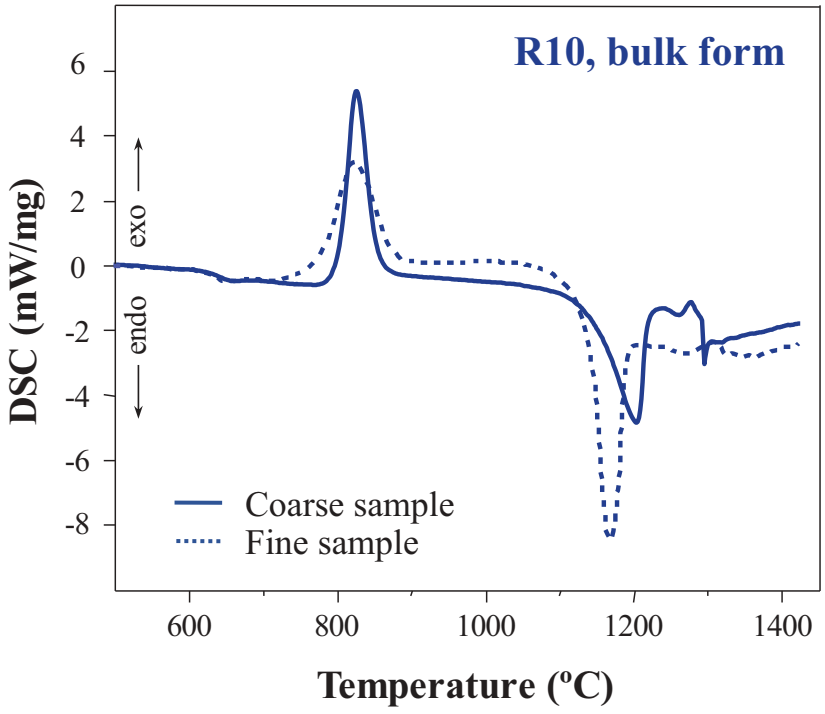

Figure 2. DSC curves recorded from fine (< 63 μm) and coarse samples of R10 glass prepared in bulk form.

Table 2. T_{gr} and ΔT_p values determined from DSC characteristic temperatures.

Glass	Cooling	Particle size	Tg (K)	Tp (K)	Tm (K)	Tgr	ΔT_p
RE	Bulk	Powder	915	1123	1448	0.63	−229
		Fragment	933	1352	1463	0.64	
	Frit	Powder	936	1156	1448	0.65	−202
		Fragment	948	1358	1458	0.65	
R6	Bulk	Powder	928	1173	1458	0.64	−65
		Fragment	936	1238	1473	0.64	
	Frit	Powder	933	1153	1445	0.65	−181
		Fragment	943	1334	1463	0.64	
R8	Bulk	Powder	911	1119	1445	0.63	−21
		Fragment	919	1140	1456	0.63	
	Frit	Powder	923	1143	1441	0.64	−77
		Fragment	934	1220	1462	0.64	
R10	Bulk	Powder	906	1095	1440	0.63	−3
		Fragment	913	1098	1478	0.62	
	Frit	Powder	908	1085	1458	0.62	6
		Fragment	913	1079	1473	0.62	

mechanism. On the contrary, fluorine exerts high influence in the spatial position at which crystals develop in the early stage of glass devitrification. Indeed, ΔT_p in RE glass with lower fluorine content (2.12 wt.%) is highly negative denoting that first crystals grow on the surface of glass grains but ΔT_p is close to zero in R10 glass (4.39 wt.% fluorine), which imply that crystals are developed in the glass internal volume.

Consequently, the estimation of the ΔT_p and T_{gr} indicates that the devitrification of these richterite-based glasses mostly involves a surface crystallization mechanism. However, the increment offluorine content in the parent glass composition leads to a variation in the place of the first developed crystals, from surface sites to the internal volume of the glass particles.

For corroborating the preferential crystallization mechanism (surface or volume), the beginning of crystal growth was promoting by subjecting fragment samples of parent glasses prepared in bulk form (quenched) to thermal treatments at the temperature interval 800–1000ºC for 5 min and the microstructure of resulting glass-ceramic materials were observed by FESEM. Figure 3 shows a general view of the microstructure of thermally treated glasses and Table 3 collects the dimensional parameters evaluated from the FESEM observations. In Figure 3(a,b) it is clear that devitrification in RE glass initiates through a surface mechanism which in the early stage gives rise to the development of crystals at the surface of glass particle forming a crystalline shell that grows inwards. The thickness (*e*) of the crystallization shell varies in the 60–135 μm interval showing an average value of $\bar{e}$ = 120 μm, which indicates that it develops at an average rate of 24 μm/min.

In R6 (Figure 3(c,d)) and R8 glasses (Figure 3(e,f)), crystallization also begins at the glass particle surface but simultaneously, the development of spherulitic crystals in the bulk volume of glasses takes place. The thickness of the crystallization shell decreases as the fluorine content in glass composition increases. Therefore, in R6 thickness is in the 65–90 μm interval with $\bar{e}$ = 80 μm while in R8 it varies in the 46–86 μm range with $\bar{e}$ = 60 μm. Consequently, the shell crystallization range also decreases with fluorine content, showing average values of 16 μm/min and 12 μm/min in R6 and R8 glasses, respectively. Concerning spherulites, the main differentiation in their growth is relating to crystal density (number of crystals per surface unit), which significantly intensifies from an average value of 1.5 crystals/mm^2 in R6 to 37 crystals/mm^2 in R8. The observed increase in spherulites number is accompanied by a slight reduction in crystal size, from an average value of 90 μm (R6 glass) to 70 μm (R8 glass).

In R10 glass (Figure 3(g,h)) the crystallization process follows a similar trend but some differences in both crystalline shell and spherulites are observed. In this case, the shell thickness decreases down to an average value of $\bar{e}$ = 45 μm, which implies a growth rate of 9 μm/min. Regarding spherulites development, crystal density in the bulk volume highly increases until reaching a value of 2.730 crystals/mm^2 and simultaneously, crystal size is reducing down to an average diameter of 14 μm. Therefore, the microstructural analysis showed in Figure 3 corroborates that in the studied richterite-based glasses crystallization begins at glass surface but volume crystallization plays an important role as the fluorine content in glasses compositions increases.

Figure 3(a,b) evidences the lack of spherulites development in the interior of RE glass particle heat-treated at 1000ºC for 5 min. However, the DSC curve recorded from a coarse sample of RE glass prepared in bulk form shows an exothermic peak indicating a crystallization process in the internal volume that at 1000ºC should be in progress. For clarifying the development of spherulites in RE glass, fragment samples were heat treated in the 1000–1100ºC temperature interval for 5 min. X-ray diffractograms and microstructure of the resulting materials are shown in Figures 4 and 5 respectively and Table 4 collects the EDS carried out in different areas marked in Figure 5.

Figure 4 supports that thermal treatment of RE glass at 1000ºC for 5 min leads to a mainly amorphous material with slight diffraction peaks, which match with F-richterite (JPCDS file No. 25–0808) phase. The crystallization shell developed after thermal treatment of RE glas at 1000ºC for 5 min (Figure 5(a)) is comprised of tiny crystal showing a dendritic growth. EDS analyses indicate that the chemical composition of shell crystals is close to F-richterite (57.35 SiO_2, 24.03 MgO, 6.69 CaO, 7,40 Na_2O, 4.53 F_2 wt.%), although both a light increasing of SiO_2, MgO y Na_2O and a decrease in Al_2O_3 y CaO content is detected. These dissimilarities are likely due to isomorphic substitution of (Mg^{2+} + Si^{4+}) for (Al^{3+} + Al^{3+}) and of (Na^{+} + Si^{4+}) for (Al^{3+} + Ca^{2+}), very common in amphiboles [26]. The detailed observation of the residual glassy phase in the

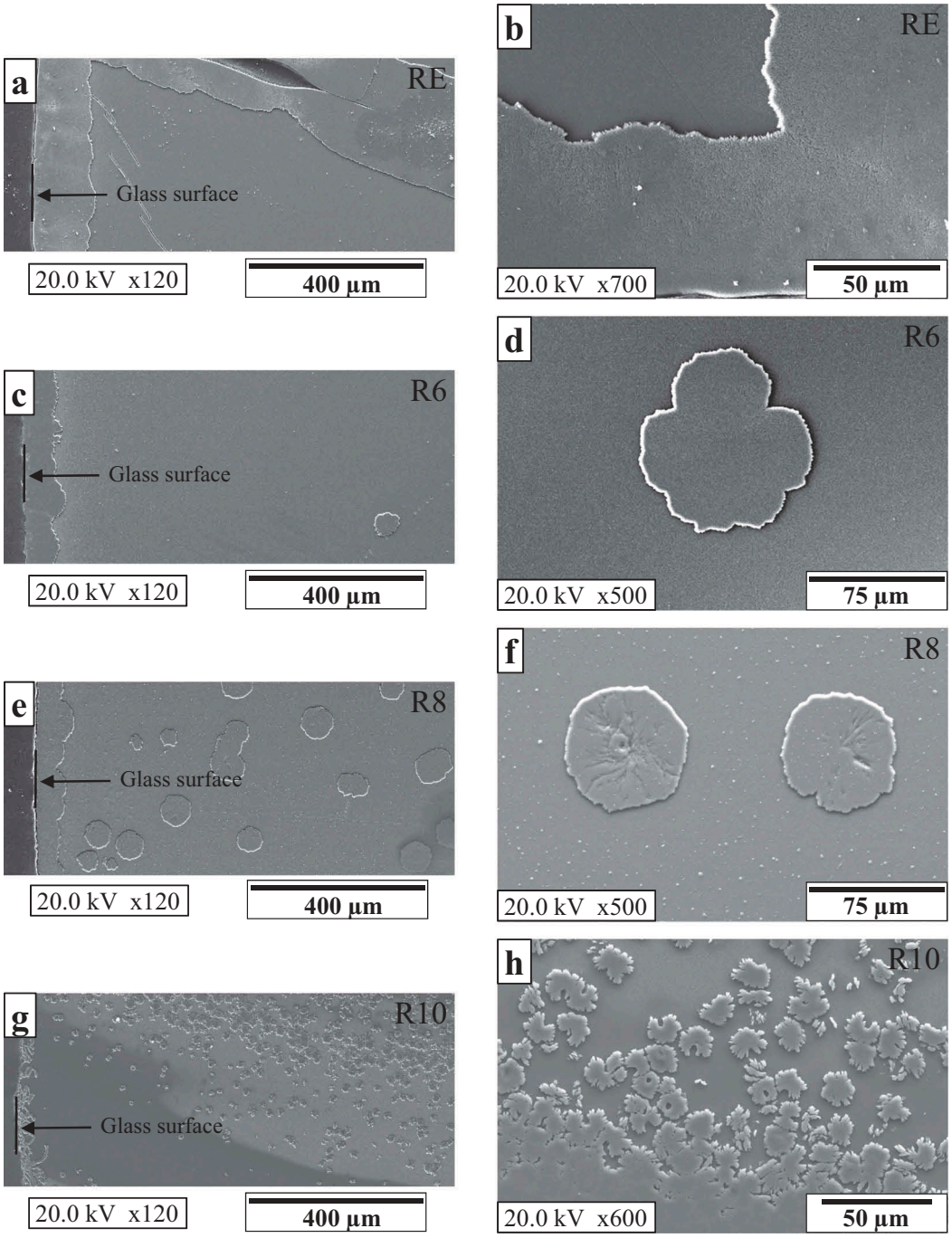

Figure 3. Secondary electron images on a cross-section of etched heat-treated glasses. a) and b) RE glass at 1000°C, 5 min; c) and d) R6 glass at 950°C, 5 min; e) and f) R8 glass at 950°C, 5 min; g) and h) R10 glass at 800°C, 5 min.

Table 3. Dimensional parameters evaluated from the FESEM observations carried out for evaluating the beginning of crystal growth.

		Crystallization shell			Espherulites	
Glass	Thermal treatment	Average thickness (µm)	Average rate (µm/min)	Crystalline phase	Crystalline density (crystals/mm^2)	Average size (µm)
RE	1000°C 5 min	120	24	Richterite	Spherulites are not detected	
R6	950°C 5 min	80	16	Richterite	1.5	90
R8	950°C 5 min	60	12	Richterite	37	70
R10	800°C 5 min	45	9	Preiswerkite Paragonite	2.730	14

material resulting from the thermal treatment of RE glass at 1000°C for 5 min (Figure 5(b)) makes clear the occurrence of tiny spherical agglomerates with an average diameter of ~ 65 nm, which should correspond to crystalline germs of bulk crystallization. The thermal treatment of RE glass at 1050°C for 5 min

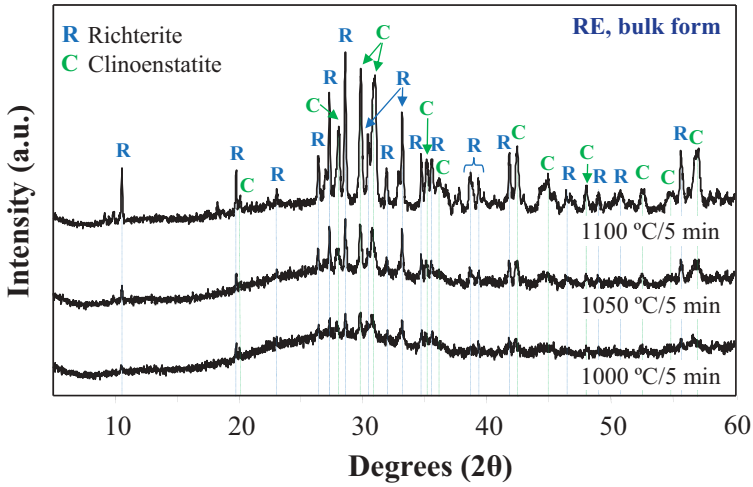

Figure 4. XRD patterns for coarse samples of RE glass prepared in bulk form after heat-treatment for 5 min in the 1000–1100°C temperature interval.

favors the development of germs, which grow and reach the average size of 500 nm. The X-ray pattern corresponding to this thermal treatment (Figure 4) allows recognizing these crystals as clinoenstatite ($MgSiO_3$, JPCDS file No. 35–0610). Thermal treatment of RE glass at 1100°C (Figure 5(e)) promotes the growth of the F-richterite crystallization shell to a greater extent but it suppresses the development of spherulites. The crystalline shell has been developed perpendicularly to the RE glass surface and it takes up the main part of the particle internal volume. Observation of RE glass thermal treated at 1100°C for 5 min at higher magnification (Figure 5(f)) shows that crystallization shell is comprised of F-richterite crystals but also including clinoenstatite crystals (Table 4), which reach an average size of 1.5 μm. EDS analyses collected from clinoenstatite crystals reveal lower MgO content together with enrichment in Al_2O_3, CaO and Na_2O compared to clinoenstatite stoichiometric composition. Clinoenstatite is a mineral belonging to pyroxene group and as amphiboles, isomorphic substitutions are recurring.

Consequently, the results point out that devitrification in RE glass begins with the development of F-richterite crystals at the glass surface. As F-richterite growth is linked to magnesium consumption, the lack of Mg^{2+} cations for the subsequent clinoenstatite crystallization is balanced out by means of their substitution by Ca^{2+} cations and by the (Al^{3+} + Na^{+}) pair [26]. Similar results are found in the devitrification study of R6 and R8 glasses.

As previously mentioned, the crystallization process of R10 glass shows some dissimilarities in the development of both crystallization shell and internal spherulitic crystals when compared with RE, R6 and R8 glasses. Figure 6 shows the microstructure of the fracture surface of the R10 glass heat-treated at 850°C for 5 min. It brings to light that the energy required for the development of crystals in the soft surface of glass should be high and thus, superficial crystallization mainly occurs through the nucleation of crystals along cracks previously existing in the parent glass (Figure 6(a,b)), where the energy requirement is lower [22,27,28].

Developed crystals, with sheet or scale shape, are arranged perpendicular to the fracture surface of cracks, giving rise to crystalline assemblages that, both because of the shape of the crystals and of their spatial arrangement, resemble micas clusters. On the other hand, devitrification in the internal volume of R10 glass develops through the precipitation of small scales or sheets, ~ 1.5 μm thick, which merge giving rise to crystalline formations with spherulite appearance (Figure 6(c)). Unlike R6 and R8 glasses, crystals developed in the inner volume of R10 glass are not properly spherulites, as needle-shaped crystals growing subparallel from a central point. In this case, it seems rather that they are straight crystals that bend in their growth and give rise to spherical or sheaf-like crystalline clusters. This type of growth has been previously reported in the study of phlogopite type mica glass-ceramics [29], in which the development of curved crystals is a consequence of the substitution of aluminum by magnesium in octahedral positions.

Figure 7 shows the X-ray pattern from R10 glass after heat treatment at 850°C for 5 min. The profile of the diffractogram indicates that after this treatment, the glass is in an initial state of its devitrification process, as is deduced by the presence of a high amorphous background on which wide peaks of crystallization overhang. X-ray pattern can be associated with the occurrence of preiswerkite ($NaMg_2Al(Si_2Al_2)O_{10}F_2$) and paragonite ($NaAl_2(Si_3Al)O_{10}F_2$) crystalline phases, both belonging to the mica group. However, semi-quantitative EDS analyses performed on the crystals of Figure 6 does not completely match the identified micas. The chemical composition of the micas is extremely variable and numerous

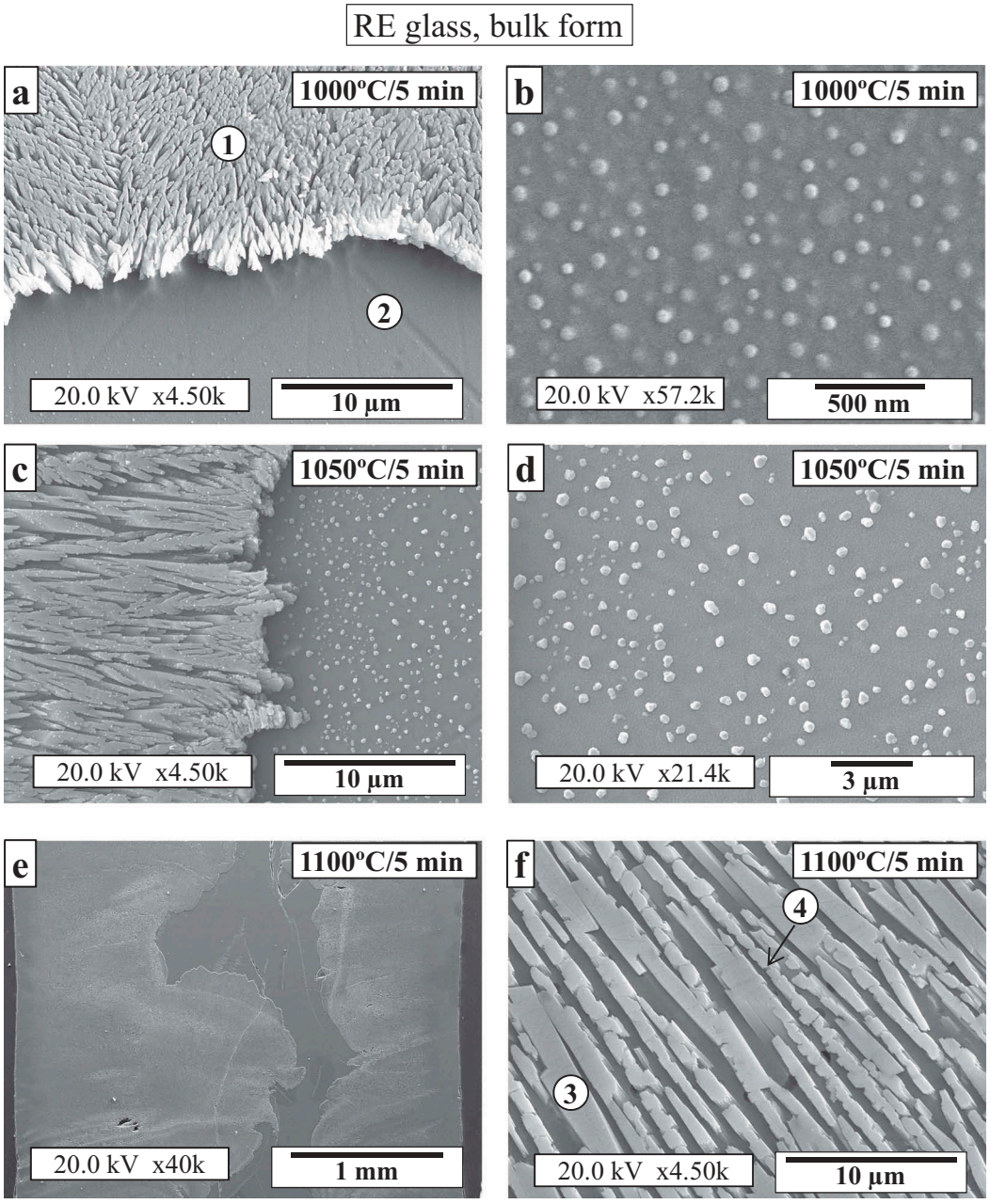

Figure 5. Secondary electron images on cross-sections of RE glass prepared in bulk form after heat treatment at a) and b) 1000ºC for 5 min; c) and d) 1050ºC for 5 min; e) and f) 1100ºC for 5 min.

Table 4. EDS analyses (wt.%) collected from crystals developed after thermal treatment of RE glass. The error is ± 0.2 wt%. Zones are marked in images in Figure 5(a,b).

Thermal treatment	Zone	Crystalline phase	SiO_2	Al_2O_3	MgO	CaO	Na_2O	F^-
1000ºC for 5 min	1	F-richterite	57.3	10.4	20.5	5.5	4.4	2.0
	2	Remaining glassy phase	57.3	11.2	17.7	5.3	7.0	1.5
1100ºC for 5 min	3	F-richterite	53.7	8.2	23.8	6.1	4.8	3.5
	4	Clinoenstatite	59.1	9.0	22.6	5.7	3.5	0.0

homo- and heterovalent isomorphic mixtures are recorded. In the case of R10 glass, these substitutions are also favored by the glass composition itself, which is scarce in alumina and it is no able to deal with the requirement of Al^{3+} cations necessary for the development of mica crystals. In this sense, Veblen [30] reported new ordered structures, called biopyriboles, which are intimately related to amphiboles. This term, derived from biotite, pyroxene, and amphibole, reflects the connection between these mineralogical phases.

The spatial layout of small crystals in the whole glass-ceramic matrix suggests that bulk crystallization in fluorrichterite glasses could progress through a phase separation process in the parent glass. For this possibility, the existence of liquid-liquid immiscibility in original glasses was observed by FESEM from original glasses (quenched) prepared in bulk form. FESEM observation were carried out on fresh fracture surfaces subjected to chemical etching (Figures 8–11). All glasses show the occurrence of phase separation and the degree of immiscibility increases with the fluorine content in glasses composition. Thus, RE

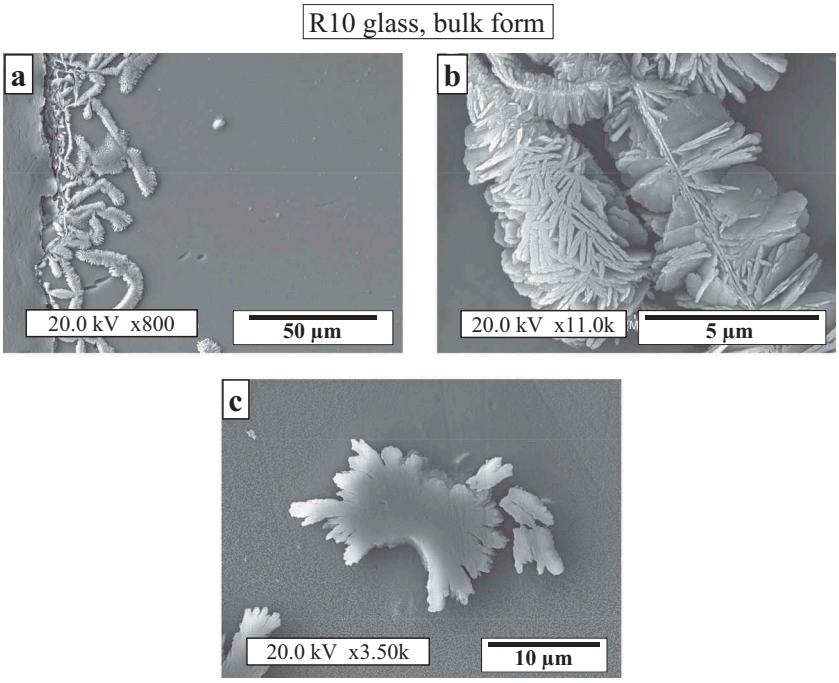

Figure 6. Secondary electron images on cross-sections of R10 glass prepared in bulk form after heat treatmentat 850ºC for 5 min. a) and b) nucleation of crystals along cracks previously existing in the parent glass; c) scales with spherulite appearance developed in the internal volume of glass particle.

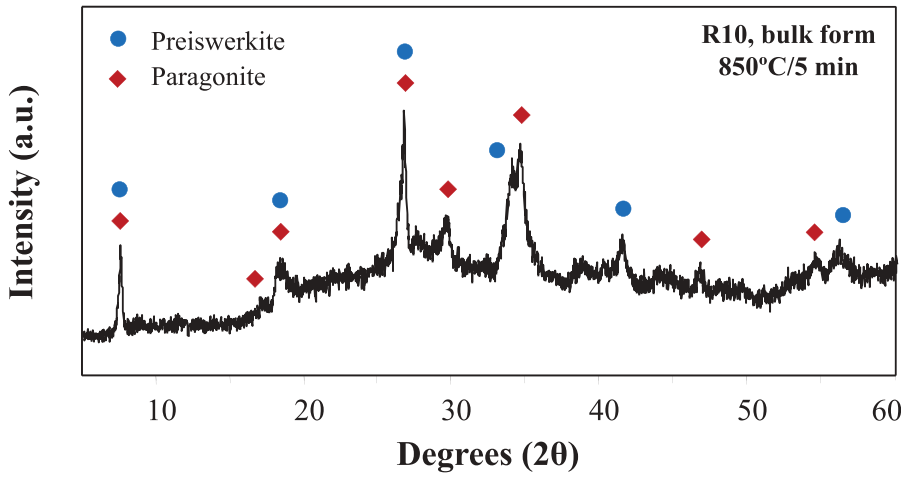

Figure 7. XRD pattern for R10 glass heat-treated at 850ºC for 5 min.

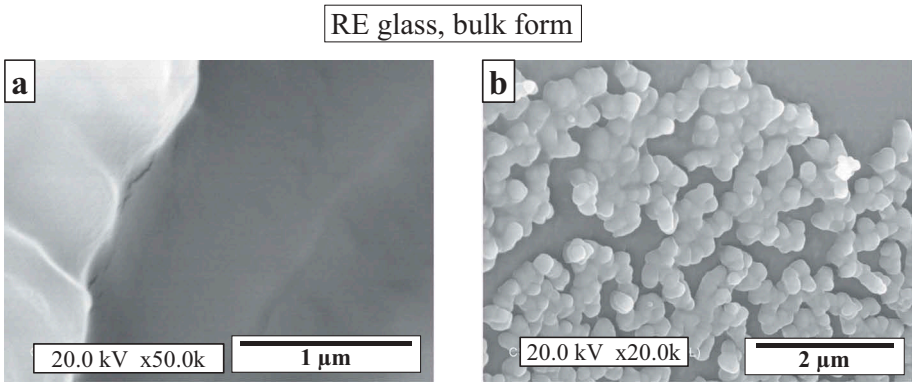

Figure 8. Secondary electron images on an etched fresh fracture of parent RE glass prepared in bulk form. a) Overview at 50 k magnification; b) agglomerates of small droplets in isolated regions observed at 20 k magnification.

glass mostly exhibits a homogeneous fracture surface (Figure 8(a)), in which a texture indicative of liquid immiscibility is not observed. However, the presence in isolated regions of agglomerates of small droplets, with a diameter comprised in the range 300–350 nm (Figure 8(b)) indicates phase separation through a nucleation and growth mechanism.

Phase separation in R6 glass is more noticeable (Figure 9(a)) and regions with different microstructure are distinguished. The observation at higher magnification (Figure 9(b)) shows that liquid-liquid immiscibility conduct to the segregation of small droplets with size within the range 40–60 nm, which in certain regions agglutinate and lead to larger aggregates (200–400 nm). The degree of phase separation in R8 glass (Figure 10) is greater than in glasses with lower fluorine content. Separation of phases clearly occurs through a nucleation and growth mechanism resulting in the formation of isolated droplets, of homogeneous size and average diameter of 175 µm.

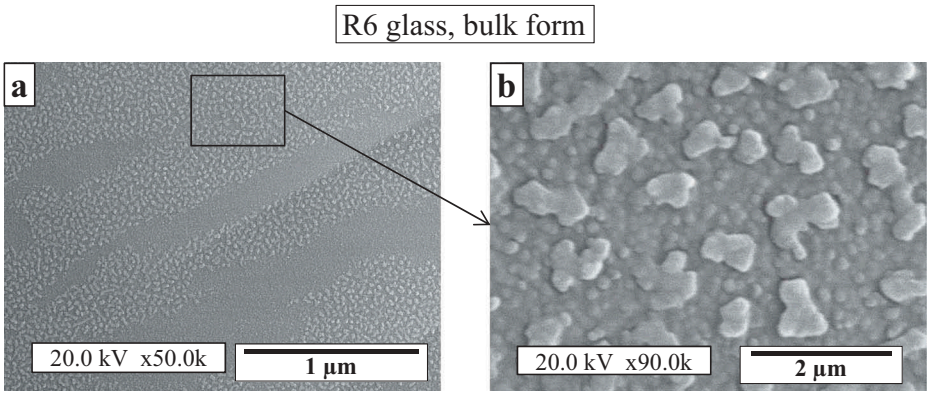

Figure 9. Secondary electron images on an etched fresh fracture of parent R6 glass prepared in bulk form. a) Overview at 50 k magnification; b) detailed observation at 90 k magnification.

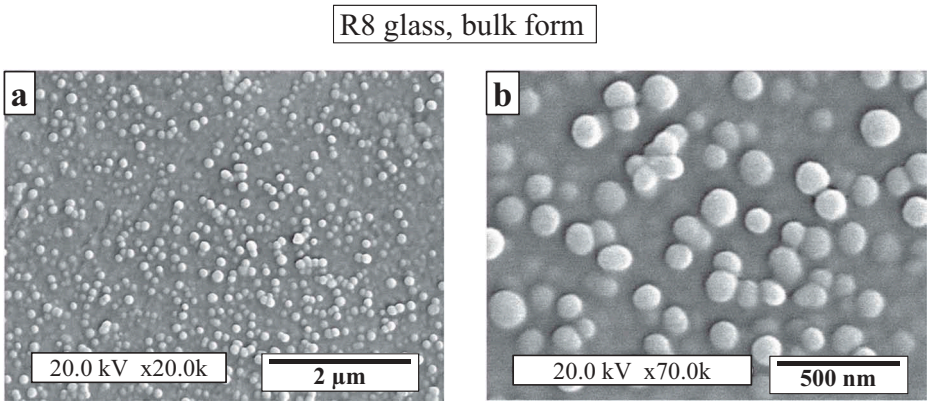

Figure 10. Secondary electron images on an etched fresh fracture of parent R8 glass prepared in bulk form. a) Overview at 50 k magnification; b) detailed observation at 70 k magnification.

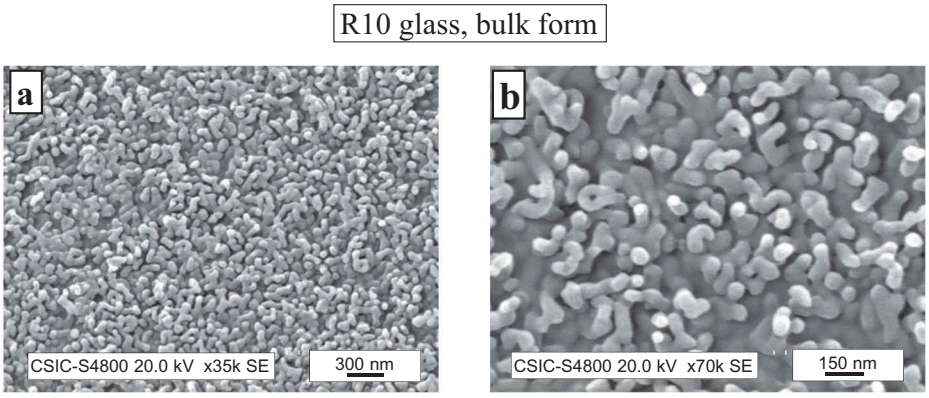

Figure 11. Secondary electron images on an etched fresh fracture of parent R10 glass prepared in bulk form. a) Overview at 35 k magnification; b) detailed observation at 70 k magnification.

Finally, a change in the development of phase separation is observed in R10 glass, which results in a spinodal decomposition mechanism (Figure 10) where phases separate as two continuous interpenetrated phases, with high connectivity and worm-like morphology. In this case, the separated phase has a maximum diameter of 125 nm in the widest part and 75 nm in the drop necks.

4. Conclusions

The crystallization of fluorrichterite-based glasses was studied by means of DSC, XRD, and FESEM. From the current results, the next conclusions can be pointed out:

- Fluorine content weakly affects the crystallization mechanism and surface crystallization mechanism is slightly prevalent.
- Fluorine exerts high influence in the spatial position at which crystals develop in the early stage of glass devitrification. In RE glass with lower fluorine content (2.12 wt.%) the first crystals grow on the surface of glass grains but in R10 glass (4.39 wt.% fluorine), crystals are developed in the glass internal volume.
- Both, the thickness and crystallization rate of the crystallization shell decreases as the fluorine content in glass composition increases.
- In RE, R6 and R8, crystallization shell is comprisedof F-richterite ($KNaCaMg_5Si_8O_{22}F_2$)crystals but also including clinoenstatite($MgSiO_3$) crystals.
- In R10 glass, crystallization shell is comprised of preiswerkite ($NaMg_2Al(Si_2Al_2)O_{10}F_2$) and paragonite ($NaAl_2(Si_3Al)O_{10}F_2$)
- Simultaneously to crystallization shell expansion, volume crystallization develops through the growth of spherulitic crystals in the bulk volume of glasses.
- Bulk crystallization in fluorrichterite glasses could progress through a phase separation process in the parent glass.

Acknowledgments

The authors would like to acknowledge Mrs. P. Díaz for her technical support in the experimental study. R. Casasola and J.M. Pérez express their gratitude to the Spanish National Research Council (CSIC) for their contract through the JAE Program (JAEPre-08-00456 and JAEDoc-08-00362, respectively), which was co-financed by the European Social Fund.

Disclosure statement

No potential conflict of interest was reported by the authors.

References

[1] Höland W, Beall GH. Glass-ceramic technology. Ohio: The American Ceramic Society; 2002.
[2] Deer WA, Howie RA, Zussman J. An introduction to the rock-forming minerals. 2nd ed. England: Pearson Eduaction Ltd; 1992.
[3] Beall GH. Chain silicate glass-ceramics. J Non-Cryst Solids. 1991;129(1–3):163–173.
[4] Denry IL, Holloway JA. Effect of magnesium content on the microstructure and crystalline phases of fluoramphibole glass-ceramics. J Biomed Mater Res. 2000;53(4):289–296.
[5] Keding R, Stachel D, Russel C. Oriented fluororichterite/diopsid glass-ceramics prepared by electrochemically induced nucleation. J Non-Cryst Solids. 2001;283(1–3):137–143.
[6] Denry IL, Holloway JA. Effect of crystallization heat treatment on the microstructure and biaxial strength of fluorrichterite glass-ceramics. J Biomed Mater Res B. 2007;80B(2):454–459.
[7] Hamzawy EMA, Abdel-Hameed SAM. Crystallization of triplet alkalies (Li, K, Na)-containing fluorrichterite glasses. Ceram Int. 2009;35(6):2139–2144.
[8] Omar AA, Hamzawy EMA, Farag MM. Crystallization of fluorcanasite-fluorrichterite glasses. Ceram Int. 2009;35(1):301–307.
[9] Hamzawy EMA, Eldera SS, Russel C. Preparation and microstructure of boron containing Mg-fluor-richterite ($Na_2Mg_6Si_8$-$xBxO_{22}F_2$) based glass-ceramics. Glass Technol-Part A. 2017;58(3):73–78.
[10] Denry IL, Holloway JA. Effect of sodium content on the crystallization behavior of fluoramphibole glass-ceramics. J Biomed Mater Res. 2002;63(1):48–52.
[11] Denry IL, Holloway JA. Elastic constants, Vickers hardness, and fracture toughness of fluorrichterite-based glass-ceramics. Dent Mater. 2004;20(3):213–219.
[12] Mirsaneh M, Reaney IM, Hatton PV, et al. Characterization of high-fracture toughness K-fluorrichterite-fluorapatite glass ceramics. J Am Ceram Soc. 2004;87(2):240–246.
[13] Bhakta S, Pattanayak DK, Takadama H, et al. Prediction of osteoconductive activity of modified potassium fluorrichterite glass-ceramics by immersion in simulated body fluid. J Mater Sci-Mater M. 2010;21(11):2979–2988.
[14] Bhakta S, Gillingham KH, Mirsaneh M, et al. In vitro biocompatibility of modified potassium fluorrichterite and potassium fluorrichterite-fluorapatite glass-ceramics. J Mater Sci-Mater M. 2011;22(9):2065–2070.
[15] Bhakta S, Faira PE, Salata LA, et al. Determination of relative in vivo osteoconductivity of modified potassium fluorrichterite glass-ceramics compared with 45S5 bioglass. J Mater Sci-Mater M. 2012;23(10):2521–2529. .
[16] Mirsaneh M, Reaney IM, James PF, et al. Effect of CaF_2 and CaO substituted for MgO on the phase evolution and mechanical properties of K-fluorrichterite glass ceramics. J Am Ceram Soc. 2006;89(2):587–595.
[17] Perez JM, Casasola R, Rincon JM, et al. Nucleation and crystallisation kinetics of a Na-fluorrichterite based glass by differential scanning calorimetry (DSC). J Non-Cryst Solids. 2012;358(20):2741–2748.
[18] Casasola R, Perez JM, Romero M. Devitrification behavior and preferred crystallization mechanism of glasses

based on fluorrichterite ($Na_2CaMg_5Si_8O_{22}F_2$) composition. Thermochim Acta. 2015;619:32–40.
[19] M. V, J. S, RE M. Refractory degradation in glass tank melters. A survey of testing methods. Cerâmica. 1997;43:180–184.
[20] Likitvanichkul S, Lacourse WC. Effect of fluorine content on crystallization of canasite glass-ceramics. J Mat Sci. 1995;30(24):6151–6155.
[21] Casasola R, Perez JM, Romero M. Glass-forming ability and thermal stability of F-phlogopite-based glasses. J Therm Anal Calorim. 2015;121(2):843–853.
[22] Zanotto ED, Fokin VM. Recent studies of internal and surface nucleation in silicate glasses (vol 361, pg 591, 2003). Philos T Roy Soc A. 2003;361 (1813):3009.
[23] Zanotto ED. Isothermal and adiabatic nucleation in glass. J Non-Cryst Solids. 1987;89(3):361–370.
[24] Zanotto ED, Weinberg MC. Trends in homogeneous crystal nucleation in oxide glasses. Phys Chem Glasses. 1989;30(5):186–192.
[25] Thakur RL, Thiagarajan S. Studies in catalyzed crystallisation of glasses: a DTA method. Cent Gass Ceram Res I B. 1966;13:33–45.
[26] Amorós JL, Barba A, Beltrán V Estructuras cristalinas de los silicatos y óxidos de las materias primas cerámicas [Crystalline structures of silicates and oxides of ceramic raw materials]. Castellón: AICE-ITC; 1994. Spanish.
[27] Schmelzer J, Moller J, Gutzow I, et al. Surface-energy and structure effects on surface crystallization. J Non-Cryst Solids. 1995;183(3):215–233.
[28] Muller R. Surface nucleation in cordierite glass. J Non-Cryst Solids. 1997;219:110–118.
[29] Höland W, Naumann K, Seifert HG, et al. Neuartige erscheinungsform von phlogopitkristallen in maschinell bearbeitbaren glaskeramiken [Novel appearance of phlogopite crystals in machinable glass ceramics]. Zeitschrift für Chemie. 1981;21:108–109.
[30] Veblen DR, Buseck PR, Burnham CW. Asbestiform chain silicates - new minerals and structural groups. Science. 1977;198(4315):359–365. German.